Primal–dual Newton interior point methods in shape and topology optimization

Ronald H. W. Hoppe, Svetozara I. Petrova

Angaben zur Veröffentlichung / Publication details:

Hoppe, Ronald H. W., and Svetozara I. Petrova. 2004. "Primal–dual Newton interior point methods in shape and topology optimization." *Numerical Linear Algebra with Applications* 11 (56): 413–29. https://doi.org/10.1002/nla.353.

Primal–dual Newton interior point methods in shape and topology optimization

R. H. W. Hoppe[1,2,*,†] and S. I. Petrova[1,3]

[1] *Institute of Mathematics, University of Augsburg, D-86159 Augsburg, Germany*
[2] *Department of Mathematics, University of Houston, Houston, TX 77204-3008, U.S.A.*
[3] *CLPP, Bulgarian Academy of Sciences, Block 25A, 1113 Sofia, Bulgaria*

SUMMARY

We consider non-linear minimization problems with both equality and inequality constraints on the state variables and design parameters as they typically arise in shape and topology optimization. In particular, the state variables are subject to a partial differential equation or systems of partial differential equations describing the operating behaviour of the device or system to be optimized. For the numerical solution of the appropriately discretized problems we emphasize the use of all-in-one approaches where the numerical solution of the discretized state equations is an integral part of the optimization routine. Such an approach is given by primal–dual Newton interior point methods which we present combined with a suitable steplength selection and a watchdog strategy for convergence monitoring. As applications, we deal with the topology optimization of electric drives for high power electromotors and with the shape optimization of biotemplated microcellular biomorphic ceramics based on homogenization modelling.

KEY WORDS: shape optimization; topology optimization; primal–dual Newton interior point methods; materials science; high power electronics; biomimetics

1. INTRODUCTION

Shape and topology optimization of devices and systems whose operating behaviour is described by partial differential equations or systems thereof is an important part of structural optimization with a very broad range of technologically relevant applications (cf. e.g. References [1–7]). These problems can be formulated as constrained optimization problems with typically non-convex objective functionals featuring both equality and inequality constraints on the state and design variables. After discretization, for instance by finite elements, one

*Correspondence to: R. H. W. Hoppe, Institute of Mathematics, University of Augsburg, University Str. 14, D-86159 Augsburg, Germany.
†E-mail: hoppe@math.uni-augsburg.de

Contract/grant sponsor: DFG-funded Collaborative Research Field SFB; contract/grant number: 438
Contract/grant sponsor: German National Science Foundation (DFG); contract/grant number: HO877/5-2
Contract/grant sponsor: Federal Ministry for Science and Technology (BMBF); contract/grant number: 03HO7AU1-8

is led to a large scale non-linear programming problem so that efficient solution techniques are much required in order to achieve optimal designs in appropriate computational times. Traditional design strategies which treat the optimization and the numerical solution of the discretized state equations separately often do not satisfy this requirement. One is usually better off with a strategy that has become known as an all-in-one approach. Here, the numerical solution of the discretized state equations is an integral part of the optimization routine which can lead to significant savings in computational time (see Section 4 below). Within the class of all-in-one approaches, primal–dual Newton interior point methods have become very popular during recent years. In this paper, we will focus on the application of these methods to some selected structural optimization problems.

The paper is organized as follows. In Section 2, we will present two optimization problems in materials science. The first one deals with the topology optimization of electric drives for high power electromotors where the design objective is to minimize parasitic inductivities caused by eddy currents. Although there is a significant amount of literature on topology optimization in mechanical applications (cf. e.g. References [1, 2] and the references cited therein), only little work has been done in the framework of electromagnetic devices and systems (see References [8–10]).

The second problem is concerned with the shape optimization of microcellular biomorphic SiC ceramics derived from natural wood by biotemplating. The design objective is to determine the microstructural geometric details in such a way that optimal performance is achieved. This is done by considering a homogenized mechanical model. We remark that the optimization of microstructured mechanical devices by the homogenization approach is well established (cf. e.g. References [1, 11] for computational aspects).

In Section 3, we give a detailed presentation of primal–dual Newton interior point methods including a discussion of the iterative solution of the primal–dual system by transforming iterations and convergence monitoring by a watchdog strategy based on a hierarchy of appropriately chosen merit functions. Finally, in Section 4, we present some numerical results for the shape and topology problems under consideration.

2. SHAPE AND TOPOLOGY OPTIMIZATION PROBLEMS

2.1. Topology optimization in high power electronics

Converter modules are pulse width modulated electronic devices used as electric drives for high power electromotors. The range of applications is from energy generation and transmission to public transportation systems such as trams and high speed trains (see, e.g. Reference [12]).

The typical configuration of a converter module is displayed in Figure 1. The module consists of semiconductor devices (insulated gate bipolar transistors (IGBTs) and gate turn off thyristors (GTOs)) serving as valves for the electric currents. They are connected with each other as well as with the power source and the load by copper made bus bars. The N bus bars occupying a bounded domain $\Omega := \bigcup_{\nu=1}^{N} \Omega_\nu \subset \mathbf{R}^3$ contain several ports $\Gamma_{\nu\alpha} \subset \Gamma = \partial\Omega$, $1 \leqslant \alpha \leqslant N_\nu$, $1 \leqslant \nu \leqslant N$, on their surfaces where currents are either supplied or taken off the bars. The IGBTs and GTOs operate at switching times of less than 100 ns and currents in the range of several kiloamperes. Due to steep current ramps, parasitic effects caused by eddy currents

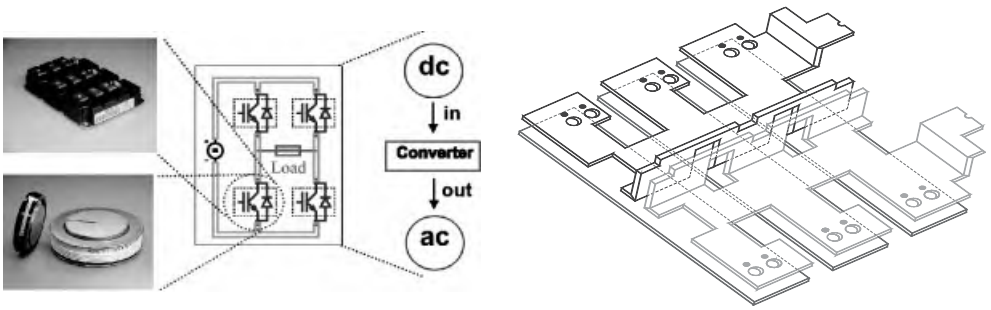

Figure 1. Converter module (left) and typical bus bars (right).

occur that lead to significant losses in the power transmission. Therefore, the designer's goal is to provide an optimal distribution of the material in such a way that the total inductivity is minimized. The total inductivity can be described by a functional

$$L(\sigma, \varphi, \mathbf{A}) := \left(\sum_{\nu,\alpha} \sum_{\mu,\beta} \int_0^T |L_{\nu\alpha,\mu\beta}(t)|^2 \, \mathrm{d}t \right)^{1/2}$$

with the generalized transient inductivity coefficients

$$L_{\nu\alpha,\mu\beta}(t) := \sigma^{-1} \int_{\Omega_\nu} f(\varphi, \mathbf{A}, t) \, \mathrm{d}x$$

where σ is the electric conductivity serving as the design parameter and f depends on the electromagnetic potentials, namely the scalar electric potential φ and the magnetic vector potential $\mathbf{A}$ which are the state variables. The design objective can thus be stated as the constrained non-linear optimization problem:

$$\inf_{\sigma,\varphi,\mathbf{A}} L(\sigma, \varphi, \mathbf{A}) \tag{1}$$

where the potentials are subject to the potential formulation of the quasistationary limit of Maxwell's equations (eddy current equations)

$$\operatorname{div}(\sigma \operatorname{grad} \varphi) = 0 \quad \text{in } \Omega \tag{2}$$

$$\sigma \mathbf{n} \cdot \operatorname{grad} \varphi = \begin{cases} -I_{\nu\alpha}(t) & \text{on } \Gamma_{\nu\alpha}, \\ 0 & \text{else} \end{cases} \tag{3}$$

$$\sigma \frac{\partial \mathbf{A}}{\partial t} + \operatorname{curl} \mu^{-1} \operatorname{curl} \mathbf{A} = \begin{cases} -\sigma \operatorname{grad} \varphi & \text{in } \Omega \\ 0 & \text{in } \mathbf{R}^3 \backslash \Omega \end{cases} \tag{4}$$

Note that μ stands for the magnetic permeability and $I_{\nu\alpha}$, $1 \leqslant \nu \leqslant N$ are the currents at the ports satisfying $\sum_{\nu,\alpha} I_{\nu\alpha}(t) = 0$.

We prescribe the total amount of material in terms of the design parameter σ which leads to the additional global constraint

$$\int_{\Omega} \sigma \, \mathrm{d}x = C \tag{5}$$

As far as the constraints for the design parameter is concerned, a natural idea would be to allow only the values $\sigma = 0$ (no material) and $\sigma = \sigma_{\max}$ (conductivity of copper). This, however, gives rise to an ill-posed 0-1 optimization problem. Therefore, we consider relaxed constraints and allow the conductivities to vary between a small positive value $\sigma_{\min} \ll 1$ and the maximum value $\sigma_{\max}$

$$\sigma_{\min} \leqslant \sigma \leqslant \sigma_{\max} \tag{6}$$

On the other hand, in order to achieve a practical design, the extreme values $\sigma_{\min}$ and $\sigma_{\max}$ should be enforced, To this end, we use a (simple isotropic material with penalization) (SIMP)-approach and scale the conductivity by means of

$$\eta(\sigma) = \left(\frac{\sigma - \sigma_{\min} + \varepsilon}{\sigma_{\max} - \sigma_{\min}} \right)^m, \quad 0 < \varepsilon \ll 1 \tag{7}$$

for some suitably chosen $m \geqslant 1$ (cf. e.g. Reference [13]). The larger the penalty parameter m is chosen, the more $\sigma_{\min}$ and $\sigma_{\max}$ are enforced.

As far as the discretization is concerned, we use the backward Euler scheme in time and the lowest order curl-conforming edge elements of Nédélec's first family (cf. Reference [14]) in space for the vector potential equation (4) both in the interior domain and in the exterior domain with an artificial boundary off the device. Equations (2) and (3) are discretized by lowest order non-conforming Crouzeix–Raviart elements. The design variable σ is discretized by elementwise constants. We emphasize that the use of edge elements and non-conforming elements prevents checkerboard patterns in the design. We refer to References [15–17] for details including multigrid and domain decomposition methods for the efficient iterative solution of the discretized state equations.

2.2. Shape optimization in biomimetics

Biomimetics is a multidisciplinary science that tries to mimic the structural composition and functionality of biological objects (see, e.g. Reference [18]). An innovative technology in biomimetics is biotemplating which stands for the material synthesis of naturally grown materials like wood into microcellular ceramic composites that are used as highly porous, temperature resistant filters in chemical processing or as catalysts in automotive applications.

Biomorphic SiC–ceramic composites are manufactured from natural wood such as pine and beech by using liquid Si infiltration, Si–gas and SiO–gas infiltration, methyltrichlorosilane (MTS) and Si–polymer infiltration (cf. e.g. References [19–21]). The biotemplating process consists of two steps: a preprocessing step involving high temperature pyrolysis and a subsequent infiltration of the carbon preform by liquid or gaseous Si based materials (cf. Figure 2).

The lengths and widths of the struts can be controlled very precisely by tuning the process parameters of the infiltration process. Therefore, the design goal is to determine these microstructural geometric details in such a way that, depending on the application, the performance of the SiC ceramics is optimized. The optimal design of microstructured devices by

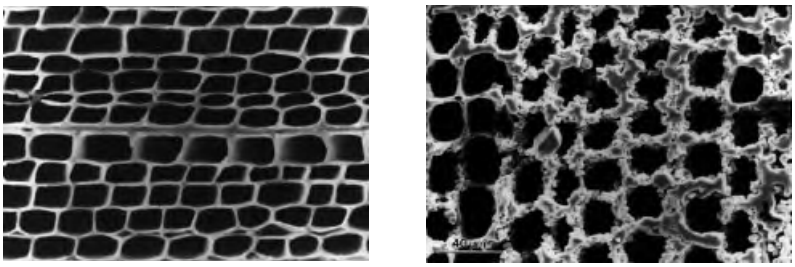

(a) (b)

Figure 2. Cellular β-SiC ceramic derived from wood: (a) pyrolized pine template, (b) Si–gas infiltrated pine (pyrolysis + infiltration at 1600° in Ar atmosphere).

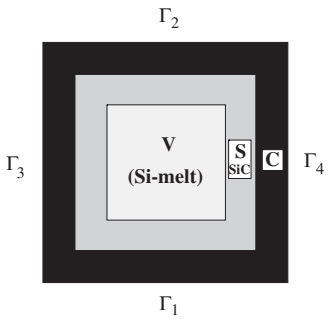

Figure 3. The periodicity cell $Y = V \cup S \cup C$.

homogenization modelling is a technique in structural mechanics that has attracted a lot of attention during the past 15 years (cf. e.g. the pioneering work [1, 2, 22] for further references). Homogenization is performed to avoid a cost-prohibitive resolution of the microstructural details. The optimal design amounts to the solution of a shape optimization problem for the homogenized model where the design variables are the lengths and widths of the different layers forming the cell walls as well as the angle of rotation (orientation of the microcells with respect to the reference frame).

For the optimal structural design, a macroscopic scale model can be provided by assuming periodically distributed cells Y consisting of an interior part treated either as a weak material or as a void (region V) surrounded by a layer of SiC (region S) and an outer layer of C (region C) (cf. Figure 3).

We assume linear elasticity and Hooke's law as the constitutive equation and denote by $\boldsymbol{E}_\alpha = (E_{\alpha ijk\ell})$ the elasticity tensor and by $\boldsymbol{\sigma}_\alpha$, $\boldsymbol{e}_\alpha$ the stress and linearized strain tensor. The homogenization approach is based on a double scale asymptotic expansion (cf. e.g. Reference [23]) and results in the homogenized elasticity tensor $\boldsymbol{E}^{\mathrm{H}} = (E^{\mathrm{H}}_{ijk\ell})$ with

$$E^{\mathrm{H}}_{ijkl} = \frac{1}{|Y|} \int_Y \left(E_{ijkl}(y) - E_{ijpq}(y) \frac{\partial \xi^{kl}_p}{\partial y_q} \right) \mathrm{d}y \tag{8}$$

The tensor $\boldsymbol{\xi} = (\xi_p^{kl})$ with periodic components $\xi_p^{kl} \in H^1_{\text{per}}(Y)$ satisfies

$$\text{div}_y(\boldsymbol{E}(y) - \boldsymbol{E}(y)\boldsymbol{e}_y(\boldsymbol{\xi}^{kl})) = \mathbf{0} \tag{9}$$

The design parameters $\boldsymbol{\alpha}$ in the structural optimization are given by the widths and lengths of the layers and the angle of orientation with respect to the reference frame. The structural optimization in terms of the state variables $\mathbf{u}$ (displacements) and the design parameters $\boldsymbol{\alpha}$ amounts to the solution of the non-linear minimization problem

$$J(\mathbf{u}, \boldsymbol{\alpha}) = \inf_{\mathbf{v}, \boldsymbol{\mu}} J(\mathbf{v}, \boldsymbol{\mu}) \tag{10}$$

subject to the constraints

$$\int_\Omega E^{\text{H}}_{ijkl} u_{k,l} v_{i,j} \, \text{d}x = \int_\Omega \mathbf{f} \cdot \mathbf{v} \, \text{d}x + \int_{\Gamma_T} \mathbf{t} \cdot \mathbf{v} \, \text{d}\sigma \tag{11}$$

$$\sum_{i=1}^{m} \alpha_i = C, \quad c_i \leqslant \alpha_i \leqslant C_i, \quad 1 \leqslant i \leqslant m \tag{12}$$

The objective functional J is chosen according to specific objectives (e.g. maximal rigidity, bending strength, etc.) and (11) refers to the homogenized elasticity equation with $\mathbf{f}$ and $\mathbf{t}$ being exterior forces. In particular, if the objective is to maximize the rigidity (minimum compliance), J is given by

$$J(\mathbf{u}, \boldsymbol{\alpha}) = \int_\Omega \mathbf{f} \cdot \mathbf{u} \, \text{d}x + \int_{\Gamma_T} \mathbf{t} \cdot \mathbf{u} \, \text{d}s \tag{13}$$

For the discretization of the cell equation (9) and the state equations (11) (homogenized elasticity equations) we use conforming P1 finite element approximations with respect to simplicial triangulations of Y and Ω (we refer to References [24–27] for details).

3. PRIMAL–DUAL NEWTON INTERIOR POINT METHODS

3.1. The general setting

The discretization of shape and topology optimization problems like those presented in Section 2 typically leads to constrained non-linear programming problems of the form

$$\min_{x \in \mathbb{R}^n} f(x) \tag{14}$$

subject to the equality constraints

$$h(x) = 0 \tag{15}$$

and the inequality constraints

$$g(x) \geqslant 0 \tag{16}$$

where $f : \mathbb{R}^n \to \mathbb{R}$, $h : \mathbb{R}^n \to \mathbb{R}^\ell$, $\ell < n$, and $g : \mathbb{R}^n \to \mathbb{R}^m$. The objective and constraint functions are assumed smooth, non-linear, and not necessarily convex.

In the applications we have in mind, typically $x=(x_1,x_2)^{\mathrm{T}}$ with $x_i\in\mathbb{R}^{n_i},\ 1\leqslant i\leqslant 2,\ n_1+n_2=n$, where x_1 represents the state variables and x_2 stands for the design parameters. We denote by

$$F:=\{x\in\mathbb{R}^n\mid h(x)=0,\ g(x)\geqslant 0\} \tag{17}$$

the feasible set and by

$$A(x):=\{1\leqslant j\leqslant m\mid g_j(x)=0\} \tag{18}$$

the so-called active set, i.e. the set of indices for which equality holds true in (16). Moreover, the set

$$G(x):=\bigcup_{j=1}^{\ell}\{\nabla_x h_j(x)\}\cup\bigcup_{j\in A(x)}\{\nabla_x g_j(x)\} \tag{19}$$

is referred to as the set of the gradients of the equality constraints and the active inequality constraints.

Coupling the constraints (15), (16) by Lagrange multipliers $y\in\mathbb{R}^{\ell}$ and $z\in\mathbb{R}^m_+$ leads to the saddle point problem

$$\min_{x\in\mathbb{R}^n}\max_{y\in\mathbb{R}^{\ell},z\in\mathbb{R}^m_+}L(x,y,z) \tag{20}$$

for the Lagrangian

$$L(x,y,z):=f(x)+y^{\mathrm{T}}h(x)-z^{\mathrm{T}}g(x) \tag{21}$$

The first-order Karush–Kuhn–Tucker (KKT) conditions are given by

$$\nabla_x L(x,y,z)=\nabla_x f(x)+\nabla_x h(x)y-\nabla_x g(x)z=0 \tag{22}$$

$$h(x)=0 \tag{23}$$

$$g(x)\geqslant 0,\quad z\geqslant 0,\quad z_j g_j(x)=0,\ 1\leqslant j\leqslant m \tag{24}$$

We remark that for $x\in F$ strict complementarity holds true if

$$z_j>0,\quad j\in A(x) \tag{25}$$

We further refer to $\nabla_x^2 f,\ \nabla_x^2 h_j,\ 1\leqslant j\leqslant\ell$, and $\nabla_x^2 g_j,\ 1\leqslant j\leqslant m$, as the Hessians of f,h_j, and g_j, respectively, and to

$$\nabla_x^2 L:=\nabla_x^2 L(x,y,z)=\nabla_x^2 f(x)+\nabla_x^2 h(x)y-\nabla_x^2 g(x)z \tag{26}$$

as the Hessian of the Lagrangian. Denoting by $J(x)$ the Jacobian of all constraints that are equal to zero at $x\in\mathbb{R}^n$ and by $N_J=N_J(x)$ a basis of the null space of $J(x)$, the matrix

$$N_J^{\mathrm{T}}\nabla_x^2 L N_J \tag{27}$$

is said to be the reduced Hessian of the Lagrangian. The second-order KKT conditions then read

$$w^{\mathrm{T}}\nabla_x^2 L w>0,\quad w\in N_J(x) \tag{28}$$

In general, the non-linear optimization problem (14)–(16) features a variety of stationary points, i.e. local minima and saddle points. The following classical result gives sufficient conditions for the existence and uniqueness of a local minimizer.

Theorem 3.1
Assume that for $x^* \in \mathbb{R}^n$ there holds

- $x^* \in F$ (feasibility),
- the vectors in $G(x^*)$ are linearly independent (regularity),
- the first-order KKT conditions (22)–(24) are satisfied,
- strict complementarity (25),
- the Hessians $\nabla_x^2 f$, $\nabla_x^2 h_j$, $1 \leqslant j \leqslant \ell$, and $\nabla_x^2 g_j$, $1 \leqslant j \leqslant m$, exist at x^* and are locally Lipschitz-continuous,
- the second-order KKT conditions (28) for the reduced Hessian are satisfied.

Then, x^* is a locally unique minimizer of (14)–(16). Moreover, there exist $y^* \in \mathbb{R}^\ell$ and $z^* \in \mathbb{R}^m$ such that (22)–(24) hold true.

Proof
We refer to Reference [28]. □

3.2. The interior point approach

Primal–dual Newton methods for the numerical solution of (14)–(16) have been intensively studied during the past decade. The idea is to use a primal–dual approach for the inequality constraints and to apply Newton's method to the first-order KKT conditions. They can be combined either with interior point methods (cf. e.g. References [29–35]) or with active set strategies (see References [36–39]). We note that for topology optimization of mechanical structures the interior point approach has been applied in Reference [40] to a convex–concave objective functional within the framework of semidefinite programming using a slightly modified MATLAB-routine for the numerical realization. The approach taken in this paper is quite different featuring a condensation of the primal–dual Hessian system with subsequent transforming null-space iterations applied to the condensed system.

The interior point approach is based on the classical logarithmic barrier functions

$$B^{(p)}(x) := f(x) - p \log g(x) \tag{29}$$

where $p \in \mathbb{R}_+$ is the barrier parameter. We are thus led to the parametrized family of equality constrained minimization subproblems

$$\min_{x \in \mathbb{R}^n} B^{(p)}(x) \text{ subject to } h(x) = 0 \tag{30}$$

Theorem 3.2
Under the conditions of Theorem 3.1, for sufficiently small barrier parameter p the optimization problem (30) admits a unique isolated local minimum $x^{(p)} \in \mathbb{R}^n$. The set $\{x^{(p)} \mid p > 0\}$ is called the barrier trajectory or central path. We have

$$x^{(p)} \to x^* \quad (p \to 0) \tag{31}$$

Proof
The reader is referred to Reference [28]. □

Denoting the Lagrangian associated with (30) by

$$L^{(p)}(x, y) := B^{(p)}(x) + y^{\mathrm{T}} h(x)$$

we consider the saddle point problem

$$\min_{x \in \mathbb{R}^n} \max_{y \in \mathbb{R}^\ell} L^{(p)}(x, y)$$

with the local solution $(x^{(p)}, y^{(p)})^{\mathrm{T}} \in \mathbb{R}^{n \times \ell}$. For the first-order KKT conditions we obtain

$$\begin{pmatrix} \nabla_x L^{(p)}(x, y) \\ \nabla_y L^{(p)}(x, y) \end{pmatrix} = \begin{pmatrix} \nabla f(x) + \nabla h(x) y - \sum_{j=1}^{m} \dfrac{p}{g_j(x)} \nabla g_j(x) \\ h(x) \end{pmatrix} = \begin{pmatrix} 0 \\ 0 \end{pmatrix} \tag{32}$$

The convergence $x^{(p)} \to x^*$ $(p \to 0)$ requires

$$y^{(p)} \to y^*, \quad \frac{p}{g_j(x^{(p)})} \to z_j^*, \quad 1 \leqslant j \leqslant m \tag{33}$$

In order to avoid ill-conditioning of the Hessian $\nabla^2 L^{(p)}(x, y)$ due to $p/g_j(x^{(p)})^2 \to \infty$, $1 \leqslant j \leqslant m$, as $p \to 0$, we introduce the auxiliary variable $z = z^{(p)} \in \mathbb{R}^m$ with

$$z_j = z_j^{(p)} := \frac{p}{g_j(x^{(p)})}, \quad 1 \leqslant j \leqslant m \tag{34}$$

which is referred to as perturbed complementarity, since by (33) it converges to the Lagrangian multiplier for (16) at optimality.

Substituting $p/g_j(x^{(p)})$ in (32) by the perturbed complementarity z_j gives rise to

$$\nabla_x L^{(p)}(x, y, z) := \nabla f(x) + \nabla h(x) y - \nabla g(x) z \tag{35}$$

with the associated first-order KKT conditions

$$F^{(p)}(x, y, z) := \nabla L^{(p)}(x, y, z) = \begin{pmatrix} \nabla f(x) + J_{\mathrm{E}}^{\mathrm{T}} y - J_{\mathrm{I}}^{\mathrm{T}} z \\ h(x) \\ D_g(x) z - pe \end{pmatrix} = \begin{pmatrix} 0 \\ 0 \\ 0 \end{pmatrix} \tag{36}$$

where J_{E} and J_{I} are the $\ell \times n$ and $m \times n$ Jacobians with respect to the equality constraints (15) and the inequality constraints (16), $D_g := \mathrm{diag}(g_j(x))_{j=1}^m$, and $e := (1, \ldots, 1)^{\mathrm{T}} \in \mathbb{R}^m$.

3.3. Newton's method and the condensed primal–dual system

Setting $\psi = (x, y, z)^{\mathrm{T}}$ and applying Newton's method to the first-order KKT conditions (36) results in the primal–dual system

$$K \Delta\psi = -F^{(p)}(\psi) \tag{37}$$

with the primal–dual matrix

$$K = \begin{pmatrix} \nabla_x^2 L^{(p)} & J_{\mathrm{E}}^{\mathrm{T}} & -J_{\mathrm{I}}^{\mathrm{T}} \\ J_{\mathrm{E}} & 0 & 0 \\ J_{\mathrm{I}} & 0 & D_z^{-1} D_g \end{pmatrix} \tag{38}$$

where $D_z := \mathrm{diag}(z_j(x))_{j=1}^m$. Since D_g is a diagonal matrix, one can easily perform block elimination of the Newton increment Δz. This leads to the condensed primal–dual system

$$\tilde{K} \begin{pmatrix} \Delta x \\ \Delta y \end{pmatrix} = - \begin{pmatrix} \nabla f(x) + J_{\mathrm{E}}^{\mathrm{T}} y - p J_{\mathrm{I}}^{\mathrm{T}} D_g^{-1} e \\ h(x) \end{pmatrix}$$

$$\tilde{K} = \begin{pmatrix} \tilde{\nabla}_x^2 L^{(p)} & J_{\mathrm{E}}^{\mathrm{T}} \\ J_{\mathrm{E}} & 0 \end{pmatrix} \tag{39}$$

with the condensed primal–dual Hessian

$$\tilde{\nabla}_x^2 L^{(p)} := \nabla_x^2 L^{(p)} + J_{\mathrm{I}}^{\mathrm{T}} D_g^{-1} D_z J_{\mathrm{I}} \tag{40}$$

3.4. Iterative solution of the condensed primal–dual system

In the sequel, we will consider in some more detail the special case that we encounter for the finite element discretized shape and topology optimization problems of Section 2. We set $x = (u, \alpha)^{\mathrm{T}}$ with the state variables $u \in \mathbb{R}^{n_1}$ and the design parameters $\alpha \in \mathbb{R}^{n_2}$ and we assume the equality constraints (15) to be of the form

$$h_1(u, \alpha) := A(\alpha) u - b \tag{41}$$

$$h_2(\alpha) := k(\alpha) - c \tag{42}$$

Here, $A(\alpha) \in \mathbb{R}^{n_1 \times n_1}$ and $b \in \mathbb{R}^{n_1}$ represent the stiffness matrix and the load vector of the discretized state equations whereas (42) with $k : \mathbb{R}^{n_2} \to \mathbb{R}$ and $c \in \mathbb{R}_+$ stands for a global equality constraint on the design parameters. Note that equality constraint (41) is, in general, non-linear with respect to the design parameters α.

As far as the inequality constraints (16) are concerned, we assume box constraints for the design parameters

$$g_1(\alpha) := \alpha - \alpha^{\min}, \quad g_2(\alpha) := \alpha^{\max} - \alpha \tag{43}$$

where $\alpha^{\min/\max} = (\alpha_1^{\min/\max}, \ldots, \alpha_{n_2}^{\min/\max})^{\mathrm{T}} \in \mathbb{R}^{n_2}$.

Denoting by $\xi = (\lambda, \eta)^{\mathrm{T}}$ with $\lambda \in \mathbb{R}^{n_1}$ and $\eta \in \mathbb{R}$ the Lagrange multipliers for the equality constraints (41) and (42) and by $z = (v, w)^{\mathrm{T}}$ with $v, w \in \mathbb{R}^{n_2}$ the perturbed complementarity for the inequality constraints (43), the condensed primal–dual system takes the form

$$\begin{pmatrix} K_{xx} & K_{x\xi} \\ K_{\xi x} & 0 \end{pmatrix} \begin{pmatrix} \Delta x \\ \Delta \xi \end{pmatrix} = - \begin{pmatrix} b_1 \\ b_2 \end{pmatrix} \tag{44}$$

with the 2×2 block matrices

$$K_{xx} := \begin{pmatrix} 0 & L_{u\alpha}^{(p)} \\ L_{\alpha u}^{(p)} & \tilde{L}_{\alpha\alpha}^{(p)} \end{pmatrix}, \quad K_{x\xi} := \begin{pmatrix} L_{u\lambda}^{(p)} & 0 \\ L_{\alpha\lambda}^{(p)} & L_{\alpha\eta}^{(p)} \end{pmatrix}, \quad K_{\xi x} = \begin{pmatrix} L_{\lambda u}^{(p)} & L_{\lambda\alpha}^{(p)} \\ 0 & L_{\eta\alpha}^{(p)} \end{pmatrix}$$

and

$$b_1 := (\nabla_u L^{(p)}, \tilde{\nabla}_\alpha L^{(p)})^{\mathrm{T}}, \quad b_2 := (\nabla_\lambda L^{(p)}, \nabla_\eta L^{(p)})^{\mathrm{T}}$$

where

$$\begin{aligned} \tilde{L}_{\alpha\alpha}^{(p)} &:= L_{\alpha\alpha}^{(p)} + D_{g_1}^{-1} D_v + D_{g_2}^{-1} D_w \\ \tilde{\nabla}_\alpha L^{(p)} &:= \nabla_\alpha L^{(p)} + D_{g_1}^{-1} \nabla_v L^{(p)} - D_{g_2}^{-1} \nabla_w L^{(p)} \end{aligned}$$

For the direct solution of the condensed primal–dual system one may use either range space methods or null space methods (cf. e.g. Reference [41]), a notion that can be adopted for iterative solvers. We use the null space formulation which can be obtained by regrouping the unknowns according to $\hat{x} = (u, \lambda)^{\mathrm{T}}$, $\hat{\xi} = (\alpha, \eta)^{\mathrm{T}}$. This leads to the linear system

$$K \Delta\varphi := \begin{pmatrix} K_{\hat{x}\hat{x}} & K_{\hat{x}\hat{\xi}} \\ K_{\hat{\xi}\hat{x}} & K_{\hat{\xi}\hat{\xi}} \end{pmatrix} \begin{pmatrix} \Delta\hat{x} \\ \Delta\hat{\xi} \end{pmatrix} = - \begin{pmatrix} \hat{b}_1 \\ \hat{b}_2 \end{pmatrix} =: d \tag{45}$$

where

$$K_{\hat{x}\hat{x}} := \begin{pmatrix} 0 & L_{u\lambda}^{(p)} \\ L_{\lambda u}^{(p)} & 0 \end{pmatrix}, \quad K_{\hat{x}\hat{\xi}} := \begin{pmatrix} L_{u\alpha}^{(p)} & 0 \\ L_{\lambda\alpha}^{(p)} & 0 \end{pmatrix}$$

$$K_{\hat{\xi}\hat{x}} := \begin{pmatrix} L_{\alpha u}^{(p)} & L_{\alpha\lambda}^{(p)} \\ 0 & 0 \end{pmatrix}, \quad K_{\hat{\xi}\hat{\xi}} := \begin{pmatrix} \tilde{L}_{\alpha\alpha}^{(p)} & L_{\alpha\eta}^{(p)} \\ L_{\eta\alpha}^{(p)} & 0 \end{pmatrix}$$

$$\hat{b}_1 := (\nabla_u L^{(p)}, \nabla_\lambda L^{(p)})^{\mathrm{T}}, \quad \hat{b}_2 := (\tilde{\nabla}_\alpha L^{(p)}, \nabla_\eta L^{(p)})^{\mathrm{T}}$$

Note that $L_{u\lambda}^{(p)} = L_{\lambda u}^{(p)} = A(\alpha)$ is the stiffness matrix and hence, the first diagonal block $K_{\hat{x}\hat{x}}$ is indefinite, but non-singular. The null space formulation (45) is solved by right transforming iterations as originally proposed in Reference [42] and applied to this kind of constrained minimization problems in References [17, 43–46]. An appropriate right transformation K^{R} is of the form

$$K^{\mathrm{R}} = \begin{pmatrix} I & 0 & -(\tilde{L}_{\lambda u}^{(p)})^{-1} L_{\lambda\alpha}^{(p)} & 0 \\ 0 & I & -(\tilde{L}_{u\lambda}^{(p)})^{-1} L_{u\alpha}^{(p)} & 0 \\ 0 & 0 & I & 0 \\ 0 & 0 & 0 & I \end{pmatrix} \tag{46}$$

Here, $\tilde{L}_{\lambda u}^{(p)}$ is a suitably chosen preconditioner for the stiffness matrix. We may use an iterative solver based on multigrid and/or domain decomposition methods (cf. e.g. References [16, 17]).

Note that K^{R} gives rise to the splitting $KK^{\mathrm{R}} = M_1 - M_2$ with $M_2 \sim 0$:

$$KK^{\mathrm{R}} = \underbrace{\begin{pmatrix} 0 & L_{u\lambda}^{(p)} & 0 & 0 \\ L_{\lambda u}^{(p)} & 0 & 0 & 0 \\ L_{\alpha u}^{(p)} & L_{\alpha\lambda}^{(p)} & \tilde{S} & L_{\alpha\eta}^{(p)} \\ 0 & 0 & L_{\eta\alpha}^{(p)} & 0 \end{pmatrix}}_{=:M_1} - \underbrace{\begin{pmatrix} 0 & 0 & L_{u\alpha}^{(p)} - L_{u\lambda}^{(p)}(\tilde{L}_{u\lambda}^{(p)})^{-1}L_{u\alpha}^{(p)} & 0 \\ 0 & 0 & L_{\lambda\alpha}^{(p)} - L_{\lambda u}^{(p)}(\tilde{L}_{\lambda u}^{(p)})^{-1}L_{\lambda\alpha}^{(p)} & 0 \\ 0 & 0 & 0 & 0 \\ 0 & 0 & 0 & 0 \end{pmatrix}}_{=:M_2}$$

where

$$\tilde{S} := \tilde{L}_{\alpha\alpha}^{(p)} - L_{\alpha u}^{(p)}(\tilde{L}_{\lambda u}^{(p)})^{-1}L_{\lambda\alpha}^{(p)} - L_{\alpha\lambda}^{(p)}(\tilde{L}_{u\lambda}^{(p)})^{-1}L_{u\alpha}^{(p)}$$

The right transforming iteration is then given by

$$\Delta\varphi^{\mathrm{new}} := \Delta\varphi^{\mathrm{old}} + K^{\mathrm{R}}M_1^{-1}(d - K\Delta\varphi^{\mathrm{old}}) \tag{47}$$

which requires the solution of a block system with the block coefficient matrix M_1 (see References [45, 46] for details). In practice, only a few numbers of such iterations are necessary to find the increments of the primal and dual variables $\Delta u, \Delta\alpha, \Delta\lambda, \Delta\eta$. The increments of v and w are then easily obtained by means of

$$\Delta v = D_{g_1}^{-1}(-\nabla_v L^{(p)} - D_v\Delta\alpha), \quad \Delta w = D_{g_2}^{-1}(-\nabla_w L^{(p)} + D_w\Delta\alpha)$$

3.5. Steplength selection and convergence monitoring

Once the Newton increments have been determined, we select suitable steplengths by computing different steplengths for primal feasibility $x = (u, \alpha)^{\mathrm{T}}$ and perturbed complementarity $z = (v, w)^{\mathrm{T}}$ whereas for dual feasibility $y = (\lambda, \eta)^{\mathrm{T}}$ we use the same steplengths as for perturbed complementarity [46]:

$$\begin{aligned} & x \mapsto x + \tau\Delta x, \quad y \mapsto y + \gamma\Delta y, \quad z \mapsto z + \gamma\Delta z \\ & \tau := \min(1, \theta\hat{\tau}), \quad \gamma := \min(1, \theta\hat{\gamma}), \quad \theta := 1 - \min(10^{-2}, 100\,p^2) \\ & \hat{\tau} := \max\{\tau \mid \alpha_j^{\min} \leqslant \alpha_j + \tau(\Delta\alpha)_j \leqslant \alpha_j^{\max},\ 1 \leqslant j \leqslant n_2\} \\ & \hat{\gamma} := \min(\hat{\gamma}_v, \hat{\gamma}_w), \quad \begin{cases} \hat{\gamma}_v := \max\{\gamma \mid v + \gamma\Delta v \geqslant 0\} \\ \hat{\gamma}_w := \max\{\gamma \mid w + \gamma\Delta w \geqslant 0\} \end{cases} \end{aligned} \tag{48}$$

Finally, an update of the dual variables is performed by solving the least-squares problem

$$\operatorname*{argmin}_y \|\nabla f(x) + L_{\mathrm{E}}^{\mathrm{T}}y - L_{\mathrm{I}}^{\mathrm{T}}z\|_2 \tag{49}$$

with L_{E} and L_{I} given by

$$L_{\mathrm{E}} := \begin{pmatrix} L_{\lambda u}^{(p)} & L_{\lambda\alpha}^{(p)} \\ 0 & L_{\eta\alpha}^{(p)} \end{pmatrix}, \quad L_{\mathrm{I}} := \begin{pmatrix} 0 & I \\ 0 & -I \end{pmatrix}$$

The convergence is tested by a watchdog strategy originally proposed in Reference [47]. We follow Reference [32] and choose a hierarchy of two merit functions, a primary merit function and a secondary merit function. The primary merit function is chosen by means of the logarithmic barrier functions and an augmented Lagrangian term with a penalty parameter $p_A > 0$ that can force the increment Δx to become a descent direction:

$$\mathscr{F}_1^{(p)}(x, y, p_A) := f(x) - p \sum_{i=1}^{2} \sum_{j=1}^{n_2} \log g_{i,j}(\alpha) + y^{\mathrm{T}} h(x) + \frac{1}{2} p_A h(x)^{\mathrm{T}} h(x)$$

where according to (41)–(43) we have

$$h(x) := (h_1(x), h_2(x))^{\mathrm{T}}, \quad h_1(x) := A(\alpha)u - b, \quad h_2(x) := k(\alpha) - c$$
$$y := (\lambda, \eta)^{\mathrm{T}}, \quad g_1(\alpha) := \alpha - \alpha^{\min}, \quad g_2(\alpha) := \alpha^{\max} - \alpha$$

The secondary merit function

$$\mathscr{F}_2^{(p)}(x, y, z) := \|F^{(p)}(x, y, z)\|_2$$

is chosen as the Euclidean norm of the residual $F^{(p)}(x, y, z)$ with respect to the first-order KKT conditions. The watchdog strategy is executed as follows. The primary merit function is tested. If it does not decrease, we switch to the secondary merit function. However, if for a maximum number of n_W iterations the primary merit function has not decreased, we choose p_A large enough to ensure progress with regard to $\mathscr{F}_1^{(p)}$.

As far as the choice of the barrier parameter p is concerned, we follow the approach suggested in Reference [32]. Depending on the number of subiterations for the line search, p is reduced rapidly close to the solution (measured in terms of the secondary merit function) and only moderately, otherwise (for details cf. also Reference [45]).

4. NUMERICAL RESULTS

In this section we report on some numerical results obtained by the application of the primal–dual Newton interior point methods, as outlined in the previous section, to the topology optimization problem in high power electronics and the shape optimization problem in biomimetics presented in Section 2.

In case of the topology optimization of converter modules, the computed design can be visualized by a grey-scale ranging from black ($\sigma = \sigma_{\max}$) to white ($\sigma = \sigma_{\min}$) which means that the black region indicates the area where material should be placed. Figure 4 displays the results in a 2D situation (3 contacts (left) and 6 contacts (right)) where the design objective is to minimize the total amount of dissipated electric energy (in both cases the penalization parameter in the SIMP-approach has been chosen as $m = 2$).

The performance of the primal–dual Newton interior point algorithm is illustrated in Table I containing the number N_{c} of contacts, the number N_{E} of elements used in the discretization, the number iter of iterations to achieve convergence, the last value of the barrier parameter p, the final values of the primary merit function $\mathscr{F}_1^{(p)}$ as well as of the secondary merit function $\mathscr{F}_2^{(p)} := \|F^{(p)}\|_2$ and the $\|z\|_2$-norm of the perturbed complementarity $z = (v, w)^{\mathrm{T}}$ at the last iteration. As stopping criterion we have used $\mathscr{F}_2^{(p)} < \mathrm{tol} := 10^{-8}$ or $p < \mathrm{tol}^2$ or $\mathrm{iter} > 100$.

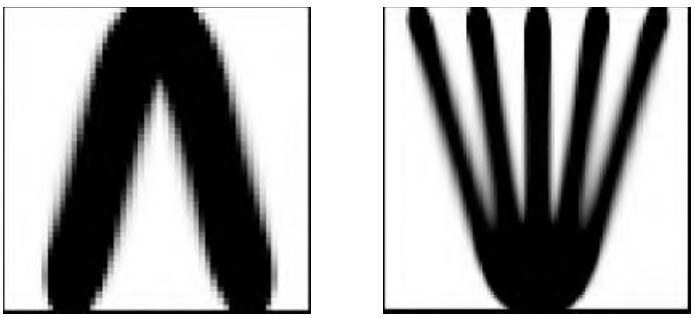

Figure 4. Material distribution: 3 contacts (left) and 6 contacts (right).

Table I. Convergence history (converter module; 2D).

N_c	N_E	iter	p	$\mathscr{F}_1^{(p)}$	$\mathscr{F}_2^{(p)}$	$\|z\|_2$
2	100	15	4.21E-17	3.57	6.94E-6	E-09
2	1200	19	1.97E-17	4.47	3.49E-5	E-09
2	1600	28	7.56E-17	4.73	3.40E-4	E-09
3	1200	33	7.03E-18	3.41	7.62E-4	E-10
3	2500	30	6.44E-19	3.78	2.40E-4	E-11
3	4200	37	3.48E-17	3.89	6.84E-4	E-10
4	900	19	3.21E-17	27.75	5.12E-5	E-10
4	3000	21	7.34E-18	27.29	8.12E-5	E-11
5	1200	19	1.56E-17	68.39	6.72E-4	E-09
5	4900	22	7.48E-18	79.14	8.45E-4	E-10
6	3000	20	9.85E-17	81.99	1.27E-3	E-09
6	4800	27	8.12E-17	84.03	5.17E-4	E-09

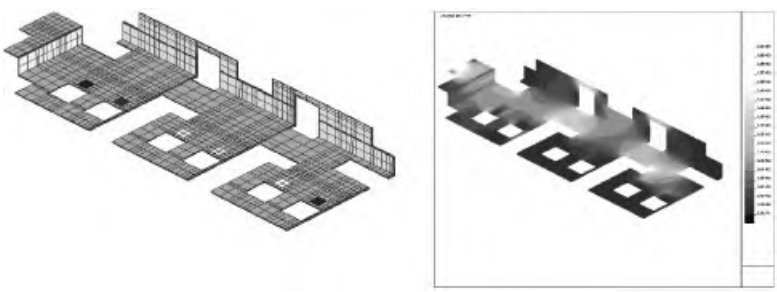

Figure 5. Optimized bus bar (left) and distribution of electric currents (right).

In the 3D case, we get similar grey-scales which have to be postprocessed to meet technological requirements (e.g. holes). Figure 5 shows the postprocessed optimal distribution of the material in a single bus bar along with a visualization of the distribution of the eddy currents.

We were able to compute a local minimum which gave rise to a reduction of the parasitic inductivities by a margin between 10 and 20% depending on the operating conditions. More-

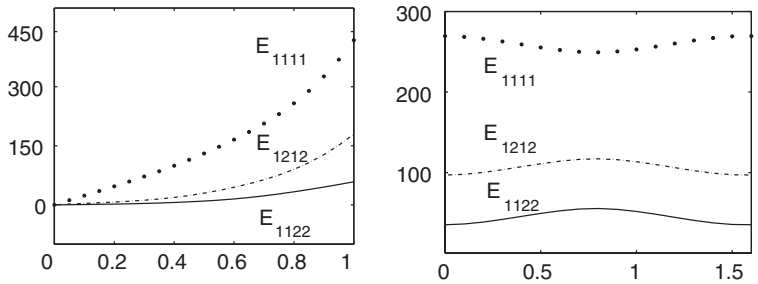

Figure 6. Homogenized elasticity coefficients w.r.t. density (left) and cell rotation (right).

Table II. Convergence history (microcellular SiC ceramics).

N_E	iter	α_1	α_2	p	$\mathscr{F}_1^{(p)}$	$\mathscr{F}_2^{(p)}$	$\|z\|_2$
40	11	4.4E-13	0.2	1.9E-13	1.33	2.9E-6	E-11
160	19	8.1E-16	0.2	2.5E-25	0.84	2.9E-8	E-13
640	14	7.7E-10	0.199	9.1E-17	0.018	2.7E-5	E-09
1048	11	4.6E-14	0.2	3.1E-22	0.53	4.5E-7	E-12
2560	11	1.9E-16	0.2	1.1E-26	0.78	6.7E-9	E-14
3712	11	3.9E-13	0.2	1.9E-10	0.49	1.5E-6	E-11
8704	11	3.7E-13	0.2	6.6E-21	0.29	1.1E-6	E-11
14 848	12	5.3E-13	0.2	8.3E-19	0.81	1.7E-6	E-11

over, compared to traditional design strategies, the primal–dual approach led to a reduction of the computational time by a factor between 20 and 30. For more details the reader is referred to References [17, 44, 45, 48].

In case of the structural optimization of biotemplated microcellular SiC ceramics, the widths and lengths of the layers (void, SiC, and C) and the angle of rotation with respect to the reference frame determine the mechanical behaviour of the workpiece. For the cell rotation, an analytical expression for the dependence of the homogenized elasticity coefficients on this design parameter is known, but for the widths and lengths of the different layers such an expression is not available. It has to be provided by computing the coefficients for different values of these design parameters and then to use multidimensional interpolation techniques. Figure 6 shows the dependence of the homogenized elasticity coefficients on the density (determined by the widths and lengths of the layers) and the angle of rotation in case of a circle as the cross section of the original wood structure. The knowledge of these dependencies then allows us to invoke the primal–dual approach described in the previous section (for details we refer to References [25–27, 46]).

Table II displays the convergence history of the primal–dual Newton interior point method where the objective is minimal compliance (maximal stiffness) in case the cell wall only consists of two layers. Again, N_E refers to the number of finite elements used for the discretization of the homogenized model, iter is the number of iterations needed for convergence, α_1 and α_2 are the computed optimal lengths of the C- and SiC-layers, p is the last value of the barrier parameter, $\mathscr{F}_1^{(p)}$ and $\mathscr{F}_2^{(p)}$ are the final values of the primary and secondary merit function

and $\|z\|_2$ is the norm of the perturbed complementarity $z=(v,w)^{\mathrm{T}}$ at the last iteration. The stopping criterion for the algorithm was the same as in the first example.

We note that in case the lower bound for α_1 is $\alpha_1^{\min}=0$, maximal stiffness is achieved, if the carbon preform completely reacts with the infiltrated silicon (i.e. if the cell wall completely consists of SiC). This is physically reasonable due to the mechanical properties of C and SiC. In this case, an alternative algorithmic approach is to symmetrize the primal–dual Hessian which practically amounts to the application of a preconditioned conjugate gradient iteration (with, e.g. incomplete Cholesky decomposition as a preconditioner) applied to the homogenized equilibrium problem.

REFERENCES

1. Bendsøe MP. *Optimization of Structural Topology*, *Shape*, *and Material*. Springer: Berlin, Heidelberg, New York, 1995.
2. Bendsøe MP, Sigmund O. *Topology Optimization*: *Theory*, *Methods and Applications*. Springer: Berlin, Heidelberg, New York, 2003.
3. Delfour MC, Zolesio J-P. *Shapes and Geometries*: *Analysis*, *Differential Calculus and Optimization*. SIAM: Philadelphia, 2001.
4. Haslinger J, Neittaanmäki P. *Finite Element Approximation for Optimal Shape Design*: *Theory and Applications*. Wiley: Chichester, 1988.
5. Mohammadi B, Pironneau O. *Applied Shape Optimization for Fluids*. Oxford University Press: Oxford, 2001.
6. Pironneau O. *Optimal Shape Design for Elliptic Systems*. Springer: Berlin, Heidelberg, New York, 1984.
7. Sokolowski J, Zolesio JP. *Introduction to Shape Optimization*. Springer: Berlin, Heidelberg, New York, 1992.
8. Gallardo JA, Lowther DA. The optimisation of electromagnetic devices using niching genetic algorithms. *COMPEL* 1999; **18**(3):285–297.
9. Seguin J, Dandurand F, Lowther DA, Sykulski JK. The optimisation of electromagnetic devices using a combined finite element/neural network approach with on–line training. *COMPEL* 1999; **18**(3):266–274.
10. Yoo J, Kikuchi N. Topology optimization in magnetic fields using the homogenization design method. *International Journal for Numerical Methods in Engineering* 2000; **48**(10):1463–1479.
11. Guedes, Kikuchi N. Pre- and postprocessing for materials based on the homogenization method with adaptive finite element methods. *Computer Methods in Applied Mechanics and Engineering* 1990; **83**:143–198.
12. Böhm P, Wachutka G, Hoppe RHW. Modelling and simulation of the transient electromagnetic behaviour of high power bus bars. In *Lecture Notes in Computational Science and Engineering*, Breuer M, Durst F, Zenger Chr (eds), vol. 21. Springer: Berlin, Heidelberg, New York, 2002; 385–392.
13. Zhou M, Rozvany GIN. The COC algorithm, part ii: topological, geometry and generalized shape optimization. *Computer Methods in Applied Mechanics and Engineering* 1991; **89**:309–336.
14. Nédélec J. Mixed finite elements in $\mathbb{R}^3$. *Numerische Mathematik* 1980; **35**:315–341.
15. Böhm P, Hoppe RHW, Mazurkevitch G, Petrova SI, Wachutka G, Wolfgang E. Optimal design of high power electronic devices by topology optimization. In *Mathematik—Schlüsseltechnologie für die Zukunft. Verbundprojekte zwischen Mathematik und Industrie*. Springer: Berlin, Heidelberg, New York, 2003; 365–376.
16. Hoppe RHW. Adaptive domain decomposition techniques in electromagnetic field computation and electrothermomechanical coupling problems. In *Proceedings of the 4th European Conference on Numerical Mathematics and Advanced Applications, ENUMATH 2001*, Brezzi F, Buffa A, Corsaro S, Almerico M (eds). Springer: Berlin, Heidelberg, New York, 2003; 201–218.
17. Hoppe RHW, Petrova SI, Schulz V. 3D structural optimization in electromagnetics. In *Proceedings of the 13th International Conference on Domain Decomposition Methods*, Debit N *et al.* (eds). CIMNE: Barcelona, Spain, 2002; 479–486.
18. Elices M. (ed). *Structural Biomaterials*. Princeton University Press: Princeton, NJ, 2000.
19. Greil P, Lifka T, Kaindl A. Biomorphic cellular silicon carbide ceramics from wood: I. Processing and microstructure. *Journal of European Ceramic Society* 1998; **18**:1961–1973.
20. Greil P, Lifka T, Kaindl A. Biomorphic cellular silicon carbide ceramics from wood: II. Mechanical properties. *Journal of European Ceramic Society* 1998; **18**:1975–1983.
21. Vogli E, Mukerji J, Hoffmann C, Kladny R, Sieber H, Greil P. Conversion of cellular silicon carbide ceramic by vapour phase reaction with SiO. *Journal of the American Ceramic Society* 2001; **84**:1236–1240.
22. Bendsøe MP, Kikuchi N. Generating optimal topologies in structural design using a homogenization method. *Computer Methods in Applied Mechanics and Engineering* 1988; **71**:197–224.

23. Jikov VV, Kozlov SM, Oleinik OA. *Homogenization of Differential Operators and Integral Functionals*. Springer: Berlin, Heidelberg, New York, 1994.
24. Hoppe RHW. Shape and topology optimization in materials science. In *Proceedings of the International Conference on Computational Mathematics* (*ICCM*-2002), Mikhailov GA, Il'in VP, Laevsky YM (eds). ICM & MG Publisher: Novosibirsk, 2002; 17–31.
25. Hoppe RHW, Petrova SI. Structural optimization of biomorphic microcellular ceramics by homogenization approach. In *Lecture Notes in Computer Science*, Margenov S, Wasniewski J, Yalamov P (eds), vol. 2179. Springer: Berlin, Heidelberg, New York, 2001; 353–360.
26. Hoppe RHW, Petrova SI. Homogenized elasticity solvers for biomorphic microcellular ceramics. In *Proceedings of the 4th European Conference on Numerical Mathematics and Advanced Applications, ENUMATH 2001*, Brezzi F, Buffa A, Corsaro S, Almerico M (eds). Springer: Berlin, Heidelberg, New York, 2003; 371–380.
27. Hoppe RHW, Petrova SI. Optimal structural design of biomorphic composite materials. In *Lecture Notes in Computer Science*, Dimov I, Lirkov I, Margenov S, Zlatev Z (eds), vol. 2542. Springer: Berlin, Heidelberg, New York, 2003; 479–487.
28. Fiacco AV, McCormick GP. *Nonlinear Programming. Sequential Unconstrained Minimization Techniques*. SIAM: Philadelphia, 1990.
29. El-Bakry AS, Tapia RA, Tsuchiya T, Zhang Y. On the formulation of the Newton interior-point method for non-linear programming. *Journal of Optimization Theory and Applications* 1996; **89**(3):507–541.
30. Wright MH. *Primal–Dual Interior–Point Methods*. SIAM: Philadelphia, 1996.
31. Forsgen A, Gill PE. Primal–dual interior methods for nonconvex non-linear programming. *SIAM Journal on Optimization* 1998; **8**(4):1132–1152.
32. Gay DM, Overton ML, Wright MH. A primal–dual interior method for nonconvex non-linear programming. *Advances in Nonlinear Programming*, Yuan Y (ed.). Kluwer: Dordrecht, 1998; 31–56.
33. Wright MH. Ill-conditioning and computational error in interior methods for non-linear programming. *SIAM Journal on Optimization* 1998; **9**(1):84–111.
34. Byrd RH, Hribar ME, Nocedal J. An interior point algorithm for large scale non-linear programming. *SIAM Journal on Optimization* 1999; **9**(4):877–900.
35. Byrd RH, Gilbert JC, Nocedal J. A trust region method based on interior point techniques for non-linear programming. *Mathematical Programming A* 2000; **9**:149–185.
36. Bergounioux M, Haddou M, Hintermüller M, Kunisch K. A comparison of a Moreau–Yosida based active strategy and interior point methods for constrained optimal control problems. *SIAM Journal on Optimization* 2000; **11**(2):495–521.
37. Bergounioux M, Kunisch K. Active set strategy for constrained optimal control problems: the finite dimensional case. In *Lecture Notes in Economics and Mathematical Systems*, Nguyen VH, Strodiot J-J, Tossings P (eds), vol. 481. Springer: Berlin, Heidelberg, New York, 2000; 36–55.
38. Bergounioux M, Kunisch K. Primal–dual strategy for state-constrained optimal control problems. *Computational Optimization and Applications* 2002; **22**(2):193–224.
39. Hintermüller M, Ito K, Kunisch K. The primal–dual active set strategy as a semi-smooth Newton method. *SIAM Journal on Optimization* 2003; **13**(3):865–888.
40. Ben-Tal A, Kočvara M, Nemirovski A, Zowe J. Free material design via semidefinite programming: the multiload case with contact conditions. *SIAM Review* 2000; **42**(4):695–715.
41. Gill PE, Murray W, Wright MH. *Practical Optimization*. Academic Press: London, 1981.
42. Wittum G. On the convergence of multigrid methods with transforming smoothers. Theory with applications to the Navier–Stokes equations. *Numerische Mathematik* 1989; **57**:15–38.
43. Maar B, Schulz V. Interior point multigrid methods for topology optimization. *Structural Optimization* 2000; **19**:214–224.
44. Hoppe RHW, Petrova SI, Schulz V. Topology optimization of high power electronic devices. In *International Series of Numerical Mathematics*, Leugering G, Hoffmann H-H (eds), vol. 139. Birkhäuser: Basel, 2002; 119–131.
45. Hoppe RHW, Petrova SI, Schulz V. A primal–dual Newton-type interior-point method for topology optimization. *Journal of Optimization Theory and Applications* 2002; **114**(3):545–571.
46. Hoppe RHW, Petrova SI. Homogenization design method for biomorphic composite materials. *Journal of Computational Methods in Science and Engineering* 2003; **3**(3):383–391.
47. Chamberlain RM, Lemaréchal C, Pedersen HC, Powell MJD. The watchdog technique for forcing convergence in algorithms for constrained optimization. *Mathematical Programming Study* 1982; **16**:1–17.
48. Hoppe RHW, Petrova SI, Schulz V. Topology optimization of conductive media described by Maxwell's equations. In *Lecture Notes in Computer Science*, Vulkov L, Wasniewski J, Yalamov P (eds), vol. 1988. Springer: Berlin, Heidelberg, New York, 2001; 414–422.